LOS ALAMOS SCIENTIFIC LABORATORY
of the
University of California
LOS ALAMOS • NEW MEXICO

Comparison of Calculations with Integral Experiments for Plutonium and Uranium Critical Assemblies

UNITED STATES
ATOMIC ENERGY COMMISSION
CONTRACT W-7405-ENG. 36

This report expresses the opinions of the author or authors and does not necessarily reflect the opinions or views of the Los Alamos Scientific Laboratory.

Printed in the United States of America. Available from Clearinghouse for Federal Scientific and Technical Information National Bureau of Standards, U. S. Department of Commerce Springfield, Virginia 22151

Price: Printed Copy $3.00; Microfiche $0.65

Written: August 1968
Distributed: October 27, 1969

LA-3529
UC-34, PHYSICS
TID-4500

LOS ALAMOS SCIENTIFIC LABORATORY
of the
University of California
LOS ALAMOS • NEW MEXICO

Comparison of Calculations with Integral Experiments for Plutonium and Uranium Critical Assemblies

by

C. C. Cremer

R. E. Hunter*

J.-J. H. Berlijn**

D. R. Worlton

*Work begun while a LASL Staff Member, completed while in capacity of Consultant. Present address: Physics Department, Valdosta State College, Valdosta, Georgia.

**Present address: Physics Department, Valdosta State College, Valdosta, Georgia.

CONTENTS

COMPARISON OF CALCULATIONS WITH INTEGRAL EXPERIMENTS FOR PLUTONIUM AND URANIUM CRITICAL ASSEMBLIES

by

C. C. Cremer, R. E. Hunter, J.-J. H. Berlijn, and D. R. Worlton

ABSTRACT

Results of comparisons of calculated and experimental values of integral experiments involving neutron cross sections of ^{235}U, ^{238}U, ^{239}Pu, and ^{240}Pu are presented. These comparisons were made in an effort to obtain microscopic neutron cross sections that would yield correct results when used in neutronics calculations of fast critical assemblies.

I. INTRODUCTION

In this report, we present the results of comparisons of calculated and experimental values of integral experiments involving the neutron cross sections of uranium and plutonium isotopes. The purpose of the program was to evolve sets of microscopic cross sections for ^{235}U, ^{238}U, ^{239}Pu, and ^{240}Pu that when used as input to neutronic calculations of fast critical assemblies would yield correct values of the assembly parameters.

The results of these calculations were used to adjust the "best fits" to the microscopic neutron cross sections, and these new "best fits" were then used to recalculate the various integral experiments. In nearly all cases the adjustments made in the course of these iterations were well within the experimental errors of the microscopic data. The notable exception is the final choice of the radiative capture cross section for ^{238}U which is discussed in detail in several sections of this report.

Integral experiments used in these comparisons were bare and reflected critical assemblies, spectral indices, neutron leakage spectra, and central core replacement measurements. We tried to produce "best fits" to the microscopic data so that a reasonable agreement was obtained for all of these types of integral results.

Calculational procedures and studies of convergence of the numerical equations and approximations used in the calculations are discussed in Sec. II.

The final choices of microscopic data were presented in two earlier reports.[1,2] Except for the radiative capture cross section for ^{238}U, those curves are not reproduced here.

II. CALCULATIONAL PROCEDURES

The one-dimensional Boltzmann transport equation can be written as

$$S(E,r,\mu,t) = \frac{1}{v}\frac{d\varphi(\mu,r,E,t)}{dt} + \nabla\cdot\left[\varphi(\mu,r,E,t)\vec{\Omega}\right] + \sigma(r,E)\varphi(\mu,r,E,t), \quad (1)$$

where v is the neutron speed at energy E,

$\varphi(\mu,r,E,t)$ is the time-dependent neutron flux,

$\vec{\Omega}$ is the direction vector of the neutron velocity,

μ is the cosine of the angle between the neutron velocity and r, and

σ is the total macroscopic cross section. $S(E,r,\mu,t)$ is the neutron source function, and can be written as a sum of terms representing fission, elastic and nonelastic processes, and a source independent of the flux:

$$S(E,r,\mu,t) = S_f(E,r,t) + S_s(E,r,\mu,t) + S_o(E,r,\mu,t). \quad (2)$$

The first three terms on the right-hand side of Eq. (2) can be written in terms of various microscopic quantities. The fission source is given by

$$S_f(E,r,t) = \tfrac{1}{2}\int_o^\infty \nu(E',r)\phi(E',r,t)\sigma_f(E',r)X(E'\to E)dE', \quad (3)$$

where $\nu(E',r)$ is the average number of neutrons per fission at energy E',

$\sigma_f(E',r)$ is the macroscopic fission cross section,

$X(E'\to E)$ is the probability that a fission occurring at energy E' gives a final-state neutron at energy E, and

$$\phi(E',r,t) = \int\varphi(\mu,r,E',t)d\mu. \quad (4)$$

The neutron-scattering source term can be written as

$$S_s(E,r,\mu,t) = \int_{-1}^{+1}\int_E^\infty \varphi(\mu,r,E',t)\sigma_s(E',r) P_s(E',\mu'\to E,\mu)dE'd\mu', \quad (5)$$

where $P_s(E',\mu'\to E,\mu)$ is the probability that a scattering process occurring at energy E' and scattering angle whose cosine is μ' results in a final-state neutron at E and μ.

The scattering source term represents elastic and nonelastic collisions including (n,n'), (n,2n), (n,3n), (n,n'f), and (n,2nf). For elastic scattering, the transfer function, P_s^e, is defined as

$$P_s^e(E',\mu'\to E,\mu) = \frac{\sigma_e(E,\mu_o)}{\sigma_e(E)}\,\delta\left[E - \frac{E'(A^2+2A\bar{\mu}_o+1)}{(A+1)^2}\right], \quad (6)$$

where μ_o and $\bar{\mu}_o$ are cosines of the scattering angles in the laboratory and center-of-mass systems, respectively,

A is the atomic mass of the nuclide,

$\sigma_e(E,\mu_o)$ is the differential scattering cross section, and

$\sigma_e(E)$ is the total scattering cross section.

For nonelastic processes we have not attempted to include any energy-angle correlation. Thus, the transfer function is defined as

$$P_s^i(E',\mu'\to E,\mu) = f_i(E'\to E)g(E',\mu'\to\mu). \quad (7)$$

g is an angular distribution function that holds for all secondary neutrons, independent of their final energy.

S_s can be expanded in terms of Legendre polynomials to give

$$S_s(E,r,\mu,t) = \int_E^\infty \sigma_s(E',r)\sum_{\ell=0}^{\infty}\phi^\ell(E',r,t) F_s^\ell(E',E)P_\ell(\mu)dE', \quad (8)$$

where $P_\ell(\mu)$ is the Legendre polynomial of order ℓ, and

$$\phi^\ell(E',r,t) = \int_{-1}^{+1}\varphi(\mu',r,E',t)P_\ell(\mu')d\mu'. \quad (9)$$

It can be shown that the scattering coefficients, F_s^ℓ, are

$$F_s^\ell(E',E) = \frac{2\ell+1}{2}\int_{-1}^{+1}P_s(E',\mu'\to E,\mu)P_\ell(\mu_o)d\mu_o. \quad (10)$$

We now integrate Eq. (1) with respect to E between E_g^- and E_g^+, which are the energy group boundaries, yielding

$$S_g(\mu,r,t) = \frac{1}{v_g}\frac{d\varphi_g(\mu,r,t)}{dt} + \nabla\cdot\left[\varphi_g(\mu,r,t)\vec{\Omega}\right] + \sigma_g(r)\varphi_g(\mu,r,t), \quad (11)$$

where

$$v_g = \frac{\int_{E_g^-}^{E_g^+}\varphi(\mu,r,E,t)dE}{\int_{E_g^-}^{E_g^+}\frac{1}{v}\varphi(\mu,r,E,t)dE}, \quad (12)$$

$$\varphi_g(\mu,r,t) = \int_{E_g^-}^{E_g^+}\varphi(\mu,r,E,t)dE, \quad (13)$$

$$\sigma_g(r) = \frac{\int_{E_g^-}^{E_g^+}\varphi(\mu,r,E,t)\sigma(E,r)dE}{\int_{E_g^-}^{E_g^+}\varphi(\mu,r,E,t)dE}, \quad (14)$$

and

$$S_g(\mu,r,t) = \int_{E_g^-}^{E_g^+}S(E,r,\mu,t)dE. \quad (15)$$

Equation (15) can be written as

$$S_g = S_g^f + S_g^s + S_g^o , \tag{16}$$

where

$$S_g^f = \int_{E_g^-}^{E_g^+} \sum_{g'=1}^{G} \int_{E_{g'}^-}^{E_{g'}^+} \nu(E',r)\phi(E',r,t)\sigma_f(E',r) \chi(E'\rightarrow E)dE'dE. \tag{17}$$

G is the number of energy groups; the group index begins at g' = 1 for the highest energy group.

$$S_g^s = \int_{E_g^-}^{E_g^+} S_s(E,\mu,r,t)dE$$

$$= \int_{E_g^-}^{E_g^+} \sum_{h=1}^{g} \int_{E_h^-}^{E_h^+} \sigma_s(E,r) \sum_{\ell=0}^{\infty} \phi^\ell(E',r,t) F_s^\ell(E',E)P_\ell(\mu)dE'dE. \tag{18}$$

Equation (18) can be rewritten by interchanging orders of integration and summation to give

$$S_g^s = \sum_{h=1}^{g} \sum_{\ell=0}^{\infty} \frac{2\ell+1}{2} \left[\sigma_{h,g}^\ell(r)\right]_s \bar{\phi}_h^\ell(r,t)P_\ell(\mu), \tag{19}$$

where

$$\bar{\phi}_h^\ell(r,t) = \int_{E_h^-}^{E_h^+} \phi^\ell(E',r,t)dE', \tag{20}$$

and

$$\left[\sigma_{h,g}^\ell(r)\right]_s = \frac{\frac{2}{2\ell+1} \int_{E_g^-}^{E_g^+} \int_{E_h^-}^{E_h^+} \sigma_s(E,r)\phi^\ell(E',r,t)F_s^\ell(E',E)dE'dE}{\bar{\phi}_h^\ell(r,t)} . \tag{21}$$

The $\left[\sigma_{h,g}^\ell(r)\right]_s$ are the ℓ^{th} momente of the group-scattering cross sections, with ϕ^ℓ serving as the weighting function.

Equation (17) also can be rewritten as

$$S_g^f = \chi_g \sum_{g'=1}^{G} (\nu\sigma_f)_{g'}\bar{\phi}_{g'}, \tag{22}$$

where

$$\bar{\phi}_g = \int_{E_g^-}^{E_g^+} \phi(E',r,t)dE', \tag{23}$$

$$(\nu\sigma_f)_g = \frac{\int_{E_g^-}^{E_g^+} \nu(E',r)\phi(E',r,t)\sigma_f(E',r)dE'}{\bar{\phi}_g} , \tag{24}$$

and

$$\chi_g = \frac{1}{\sum_{g'=1}^{G} (\nu\sigma_f)_{g'}\bar{\phi}_{g'}} \sum_{g'=1}^{G} \int_{E_{g'}^-}^{E_{g'}^+} \nu(E',r)\phi(E',r,t)\sigma(E',r) \left[\int_{E_g^-}^{E_g^+} \chi(E'\rightarrow E)dE\right] dE'. \tag{25}$$

For calculation of $\sigma_{h,g}^\ell$, χ_g, and $(\nu\sigma_f)_g$, the functions $\phi^\ell(E',r,t)$ and $\bar{\phi}(E',r,t)$ appearing in Eqs. (21), (24), and (25) were replaced by a single weighting function, W(E).

The Boltzmann transport equation, Eq. (11), can then be written as

$$\frac{1}{v_g} \frac{d\varphi_g(\mu,r,t)}{dt} + \nabla\cdot\left[\varphi_g(\mu,r,t)\vec{\Omega}\right] + \sigma_g(r)\varphi_g(\mu,r,t) = \chi_g \sum_{g'=1}^{G} (\nu\sigma_f(r))_{g'}\bar{\phi}_{g'}(r,t) + \sum_{h=1}^{g} \sum_{\ell=0}^{\infty} \frac{2\ell+1}{2} \sigma_{h,g}^\ell(r) \bar{\phi}_h^\ell(r,t)P_\ell(\mu) , \tag{26}$$

where $\sigma_{h,g}^\ell(r)$ is the scattering matrix, including both elastic and nonelastic contributions. When all terms higher than ℓ = L are dropped, Eq. (26) becomes the nontransport-corrected "L-approximation."

To derive the transport correction to the Boltzmann equation, we subtract the term $\sigma_{g,g}^{L+1}(r)\varphi_g(\mu,t)$ from both sides of Eq. (26):

$$\frac{1}{v_g}\frac{d\varphi_g(\mu,r,t)}{dt} + \nabla\cdot\left[\varphi_g(\mu,r,t)\vec{\Omega}\right] + \left[\sigma_g(r) - \sigma^{L+1}_{g,g}(r)\right]\varphi_g(\mu,r,t) = \chi_g \sum_{g'=1}^{G}\left[\nu\sigma_f(r)\right]_{g'}\phi_{g'}(r,t)$$

$$+ \sum_{h=1}^{g-1}\sum_{\ell=0}^{\infty}\frac{2\ell+1}{2}\phi^{\ell}_h(r,t)\sigma^{\ell}_{h,g}(r)P_\ell(\mu) + \sum_{\ell=0}^{\infty}\frac{2\ell+1}{2}\sigma^{\ell}_{g,g}(r)\phi^{\ell}_g(r,t)P_\ell(\mu) \qquad (27)$$

$$- \sigma^{L+1}_{g,g}(r)\sum_{\ell=0}^{\infty}\frac{2\ell+1}{2}\phi^{\ell}_g(r,t)P_\ell(\mu),$$

where we have used the relation

$$\varphi_g(\mu,r,t) = \sum_{\ell=0}^{\infty}\frac{2\ell+1}{2}\phi^{\ell}_g(r,t)P_\ell(\mu). \qquad (28)$$

This yields

$$\frac{1}{v_g}\frac{d\varphi_g(\mu,r,t)}{dt} + \nabla\cdot\left[\varphi_g(\mu,r,t)\vec{\Omega}\right] + \left[\sigma_g(r) - \sigma^{L+1}_{g,g}(r)\right]\varphi_g(\mu,r,t) = \chi_g \sum_{g'=1}^{G}\left[\nu\sigma_f(r)\right]_{g'}\phi_{g'}(r,t)$$

$$+ \sum_{h=1}^{g-1}\sum_{\ell=0}^{\infty}\frac{2\ell+1}{2}\phi^{\ell}_h(r,t)\sigma^{\ell}_{h,g}(r)P_\ell(\mu) + \sum_{\ell=0}^{\infty}\frac{2\ell+1}{2}\left[\sigma^{\ell}_{g,g}(r) - \sigma^{L+1}_{g,g}(r)\right]\phi^{\ell}_g(r,t)P_\ell(\mu). \qquad (29)$$

The transport-corrected L-approximation is made by dropping all terms higher than L in Eq. (29). Note that the "in-group" term [last term in Eq. (29)] for $\ell = L+1$ is zero and that the terms dropped by the L-approximation are given by

$$\sum_{\ell=L+2}^{\infty}\frac{2\ell+1}{2}\left[\sigma^{\ell}_{g,g}(r) - \sigma^{L+1}_{g,g}(r)\right]\phi^{\ell}_g(t)P_\ell(\mu).$$

Note also that the terms dropped are proportional to ϕ^{ℓ}_g. Thus, the error introduced depends on the anisotropy of the true flux. It is interesting to examine the ratio of the terms dropped with the transport-corrected to the nontransport-corrected case:

$$R = \frac{\sum_{\ell=L+2}^{\infty}\frac{2\ell+1}{2}\left(\sigma^{\ell}_{g,g} - \sigma^{L+1}_{g,g}\right)\phi^{\ell}_g P_\ell(\mu)}{\frac{2L+3}{2}\sigma^{L+1}_{g,g}\phi^{L+1}_g P_{L+1}(\mu) + \sum_{\ell=L+2}^{\infty}\frac{2\ell+1}{2}\sigma^{\ell}_{g,g}\phi^{\ell}_g P_\ell(\mu)} \qquad (30)$$

R is greater or less than unity depending on the rate of convergence of $\sigma^{\ell}_{g,g}$; if convergence is rapid, the transport-corrected expression in the numerator of R is larger, term by term, than the denominator, owing to the presence of the quantity $\sigma^{L+1}_{g,g}$ that appears in every term in the numerator.

Let us review the assumptions made in the calculational procedures used in this report.

1. A single weighting flux is adequate for generating group cross sections for all radii.
2. The zeroth moment of the weighting flux obtained in the Legendre expansion of $\varphi(\mu,E,r,t)$ was used to obtain group cross sections of higher moments.
3. Energy-angle correlations are retained only in elastic scattering and are approximated there by a Legendre expansion of the scattering matrix.

The group cross sections described are generated by a computer code, SIGMA, which utilizes the set of equations given. The weighting flux, microscopic cross sections, and angular scattering coefficients serve as input.

The group cross sections then serve as input to a computer code, MODERN, which utilizes the discrete S_n approximation to the transport equation.[3,4]

Most of the calculations performed in this report consist of computing the reactivity, K, of a given assembly. K is determined by requiring that the term $S_{f/K}$ produce a stationary solution to the Boltzmann equation. Thus 1/K is the value by which the fission source must be scaled to bring the calculated assembly to critical.

III. CRITICAL ASSEMBLIES

Calculations were made on various integral quantities obtained from measurements on three bare homogeneous critical assemblies. These are as follows:

A. Lady Godiva[5]

Lady Godiva is a bare uranium sphere, measured

to be delayed critical with a mass of 52.25 kg at a density of 18.71 g/cm^3, corresponding to a radius of 8.736 cm. The measured isotopic composition of the enriched uranium (Oy) was 93.71 wt% ^{235}U, 5.25 wt% ^{238}U, and 1.04 wt% ^{234}U. The assembly was found to be prompt critical, i.e., without the delayed neutrons, with the addition of ΔM_c = 1.27 kg of Oy on the surface of the sphere.

B. Jezebel[6]

Jezebel is a bare plutonium sphere, measured to be delayed critical with a mass of 16.45 kg at a density of 15.818 g/cm^3, corresponding to a radius of 6.285 cm. The measured isotopic composition of the plutonium was 94.134 wt% ^{239}Pu, 4.848 wt% ^{240}Pu, and 1.018 wt% gallium. The assembly was found to be prompt critical with the addition of 113.5 g of plutonium on the surface.

C. Dirty Jezebel[7]

"Dirty Jezebel" is the name given to a critical assembly of so-called dirty plutonium; that is, plutonium that contains a relatively high percentage of ^{240}Pu. The assembly in question used plutonium with an isotopic composition of 75.24 wt% ^{239}Pu, 20.79 wt% ^{240}Pu, 2.97 wt% ^{241}Pu, and 1.00 wt% gallium. The delayed critical mass was measured to be 18.82 ± 0.06 kg, at a density of 15.76 g/cm^3.

In addition to these homogeneous assemblies, two reactor assemblies of low enrichment uranium were used. They were pseudospherical assemblies studied under the ZPR-III program[8] and designated 6F and 9A. Each consisted of a low enrichment core with a natural uranium reflector.

D. Assembly 6F

In the 6F configuration, the core composition was 14.0 vol% ^{235}U, 15.9 vol% ^{238}U, 31.4 vol% aluminum, 12.3 vol% stainless steel, and 26.4 vol% void. (The stainless steel was represented in the calculations by iron.) The mass of ^{235}U in the core was specified as 131.1 kg. A uranium density of 18.75 g/cm^3 gave a total core mass of 372.6 kg. The density of the core material was calculated to be 10.14 g/cm^3, giving a core radius of 22.852 cm.

The core was surrounded by a reflector consisting of 0.19 vol% ^{235}U, 83.30 vol% ^{238}U, 2.27 vol% aluminum, 7.31 vol% stainless steel, and 6.93 vol% void, at 17.73 g/cm^3 density. The reflector thickness was effectively infinite with respect to reactivity measurements. For calculation, thicknesses of 30 and 50 cm were used with no significant variation in the calculated reactivity.

E. Assembly 9A

The core material in the 9A assembly was specified as 11.70 vol% ^{235}U, 38.00 vol% ^{238}U, 21.50 vol% aluminum, 14.22 vol% stainless steel, and 14.58 vol% void. The mass of ^{235}U in the core was given as 146.2 kg.

A uranium density of 18.75 g/cm^3 gave a total core mass of 740.5 kg at 13.01 g/cm^3 density, corresponding to a core radius of 25.15 cm.

The reflector composition was given as 0.19 vol% ^{235}U, 83.30 vol% ^{238}U, 7.31 vol% stainless steel, and 9.20 vol% void. The density was calculated to be 18.10 g/cm^3. The thickness was taken to be 30 cm.

IV. CONVERGENCE CALCULATIONS

A. Convergence

To determine the degree of convergence of the 10-group calculations, the reactivity, k, of Lady Godiva (where k = 1.0 for a critical system) was computed for n = 4, 8, 12, and 16, where n is the number of angular zones. These calculated values can be compared with the results given by Lee[3] for a one-group test problem for which the exact solution is known. The curve of k vs n for the S_n calculations, normalized to the test problem at n = 8, is given in Fig. 1. The convergence patterns

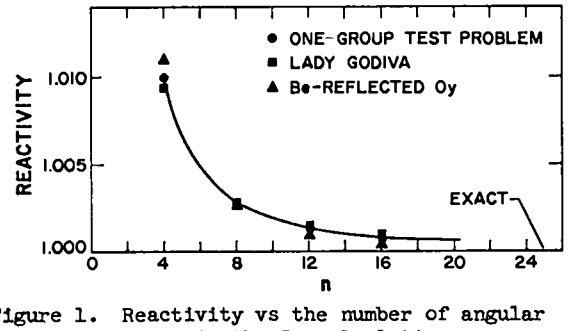

Figure 1. Reactivity vs the number of angular zones in the S_n calculations.

for the 10-group calculations of Lady Godiva and a beryllium-reflected Oy assembly are essentially the same as those for the one-group test problem. This strongly suggests that the numerical accuracy of the

calculation should be of the order of the accuracy of the test problem.

The convergence was tested as a function of the order of the Legendre expansion of the angular dependence of the scattering matrix. A set of calculations was performed for Legendre expansions up to fourth order. In addition, the effect of transport corrections was studied for P_0 and P_1 calculations. The results for Lady Godiva and a beryllium-reflected Oy assembly are plotted in Fig. 2.

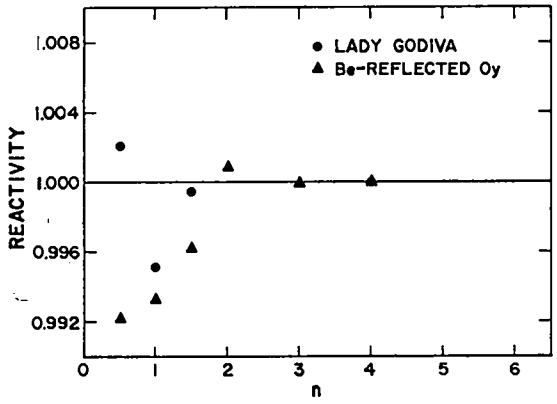

Figure 2. Reactivity vs the order of the Legendre expansion of the angular dependence of the scattering matrix.

Because the curve is flat above the third order, we assumed that the calculation has converged by that point and scaled the curve to k = 1.0 at n = 3. Because transport correction for n = 1 yields a calculation intermediate between n = 1 and n = 2, we arbitrarily plotted this calculation at n = 1.5. The S_n convergence was checked as a function of the order of the Legendre expansion. The S_n convergence pattern for P_4 calculations was not noticeably different from that given in Fig. 1.

Because of the requirements of our production codes, we normalized the cross sections used in this work to S_8, P_1 transport-corrected calculations. It can be seen that the calculational bias on S_8 is about +0.003, while that on P_1, transport corrected, ranges from -0.0005 to -0.0038. Thus, the cross sections (for uranium, at least) are normalized low; an exact calculation of Lady Godiva using the cross sections presented in Refs. 1 and 2 would presumably yield a reactivity of 0.9975. This amounts, for example, to an implied 0.25% change in $\bar{\nu}$.

The number of radial zones in the assembly material was studied. Calculations of Lady Godiva were performed using 30 and 50 radial zones. The change in reactivity was 0.00001.

B. Energy Group Spacing

Because the cross sections are averaged over energy groups with a weighting flux, we studied the question of group spacing. To take an extreme case, a beryllium-reflected, enriched-uranium assembly (see assembly No. 7, Table VI) was studied, as well as Lady Godiva. This was done to study the effect of five-group spacing over the beryllium resonance between 1 and 4 MeV.

Table I

STANDARD ENERGY GROUPS

Group	Lower Energy Boundary (MeV)	Upper Energy Boundary (MeV)
1	10.0	14.0
2	6.07	10.0
3	2.231	6.07
4	1.353	2.231
5	0.4979	1.353
6	0.1832	0.4979
7	0.0674	0.1832
8	0.0248	0.0674
9	0.00912	0.0248
10	0.000167	0.00912

Table II

TEST ENERGY GROUPS

Group	Lower Energy Boundary (MeV)	Upper Energy Boundary (MeV)
1	10.0	14.0
2	6.07	10.0
3	4.00	6.07
4	3.30	4.00
5	2.90	3.30
6	2.60	2.90
7	2.20	2.60
8	1.70	2.20
9	1.353	1.70
10	1.10	1.353
11	0.4979	1.10
12	0.1832	0.4979
13	0.0674	0.1832
14	0.0248	0.0674
15	0.00912	0.0248
16	0.00016	0.00912

The standard 10-group set used in the body of this study is listed in Table I. A 16-group test set was constructed as shown in Table II. The changes in reactivity for Lady Godiva and the reflected assembly were +0.0001 and +0.0004, respectively. This is an order of magnitude less than the correction due to S_n and P_n convergence.

In the limit of infinite groups, the weighting function cancels from the equations. From the above calculations, we feel that the particular choices of group spacing and weighting functions are not significant for the calculations in this report.

V. CRITICAL ASSEMBLY COMPARISONS

Using the cross-section data and experimental critical assembly configurations given, we calculated the reactivities of the assemblies, using the MODERN program. The calculations were performed for both the delayed-critical and prompt-critical configurations. Calculations of α_{Rossi} were also made. Table III summarizes the experimental[5,9] and calculated values for these quantities. Significant figures are quoted to the limits of experimental error.

Table III

REACTIVITY AND α_{ROSSI} COMPARISONS

Assembly Parameter	Experimental	Calculated
$k_{delayed}$:		
Lady Godiva	1.000 ± 0.001	1.000
Jezebel	1.000 ± 0.001	1.000
Dirty Jezebel	1.000 ± 0.001	1.000
ZPR-III, 6F	1.000[a]	0.995
ZPR-III, 9A	1.000[a]	0.996
k_{prompt}:		
Lady Godiva	1.000 ± 0.001	1.000
Jezebel	1.000 ± 0.001	1.000
Dirty Jezebel		1.000[b]
α_{Rossi} (μs^{-1}):		
Lady Godiva	-1.06 ± 0.03[c]	-1.19
Jezebel	-0.65 ± 0.01[d]	-0.64
Dirty Jezebel	--	-0.62

[a] No experimental uncertainties are quoted; nonsphericity and inhomogeneity effects are estimated to give an uncertainty of roughly 0.01 in k.

b. For calculated prompt critical mass of 18.948 kg.

c. Ref. 5

d. Ref. 9

All experimental values except α_{Rossi} at delayed critical mass are obtained by definition from a determination of the delayed and prompt critical configurations. The quoted experimental errors in reactivity are calculated from the experimental errors in the critical masses.

The agreement between calculated and measured reactivities ($k_{delayed}$ and k_{prompt}) is very good. The implied overall discrepancies in cross sections and other reactor parameters are less than 0.1%. This agreement is due in part to normalization, since the delayed critical reactivity was used in each case as the normalization point of the cross sections.

The disagreement between calculated and measured values for α_{Rossi} for Lady Godiva is not understood, but has been noted in previous comparisons.[10] In an effort to understand this discrepancy, we studied the behavior of α as a function of the excess reactivity above delayed critical. Mass was added to the critical Lady Godiva assembly in increments up to ΔM_c, at which point α is zero. The calculated values of α vs these mass increments (given in cents) are plotted in Fig. 3.

Also plotted in Fig. 3 are values of α at 51.9¢ and 73.9¢ which were measured with the betatron technique by Bendt et al.,[11] and a set of data obtained by Peterson[5] using passive detectors. The data were fitted with a curve which gives $\alpha = -1.06\ \mu sec^{-1}$ at 0.0¢. The probable experimental errors quoted by Bendt et al. are about ± 6%.

The calculated and experimental curves deviate uniformly, and do not agree within Bendt's quoted probable errors. This graph serves largely to confirm the lack of understanding of this disagreement.

The calculated fluxes in the assembly cores are given in Fig. 4. These fluxes were used as the weighting functions for computing group-averaged cross sections for use in the calculations. They were obtained by assuming a weighting function and calculating an assembly. The calculated flux was then used as the new weighting function. Successive

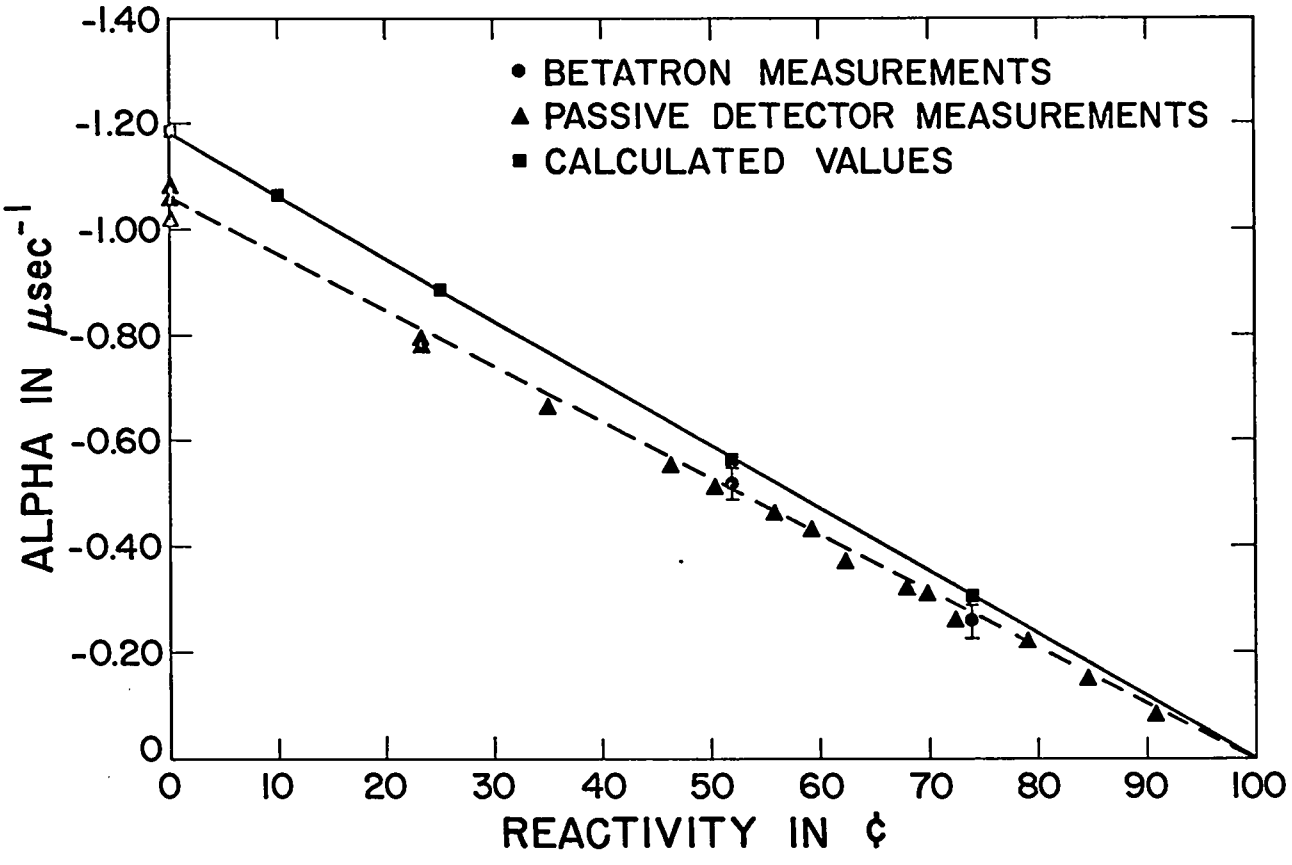

Figure 3. Rossi alpha vs excess reactivity for Lady Godiva.

iterations were performed until a stationary flux was obtained. The changes in calculated results due to these iterations were negligible.

It should be noted, with respect to the cross sections used in these calculations, that the sensitivity of the calculations to variations of the cross-section curves is a function of the neutron flux. Thus, the confidence level in the cross sections is higher in the central energy region (0.1 to 6 MeV) than at either extreme.

The leakage spectrum for Lady Godiva has been measured by Frye et al.,[12] using a nuclear emulsion technique. This spectrum and the calculated leakage spectrum flux for Lady Godiva are compared in Fig. 5. Because the computer calculations are performed with group-averaged cross sections, the leakage spectra are given in terms of averages over the various groups. The calculated curve agrees with the measured fluxes within experimental error. All data are normalized to one neutron per square centimeter over the six energy groups for which experimental data were given.

The leakage spectrum from a bare sphere of enriched uranium has also been measured by Profio et al.,[13] using a time-of-flight technique. A pulsed linac provided a source of photoneutrons at the center of the sphere. The sphere multiplication was about 20. Neutrons above about 1.5 MeV were detected by a liquid scintillator. Below 1.5 MeV, a boron capture detector was used. The absolute efficiency of each detector is believed to be known to ± 15%.

When the data from the two detectors (integrated over all angles) are plotted together, a serious discontinuity is seen to exist where the measurements overlap (Fig. 6). Since the absolute efficiency of the two detectors is much more uncertain than the relative efficiency as a function of energy in each individual detector, we applied an arbitrary scaling factor of 0.72 to bring the two measurements together in the overlap region. The data with the scale factor applied are shown in Fig. 7.

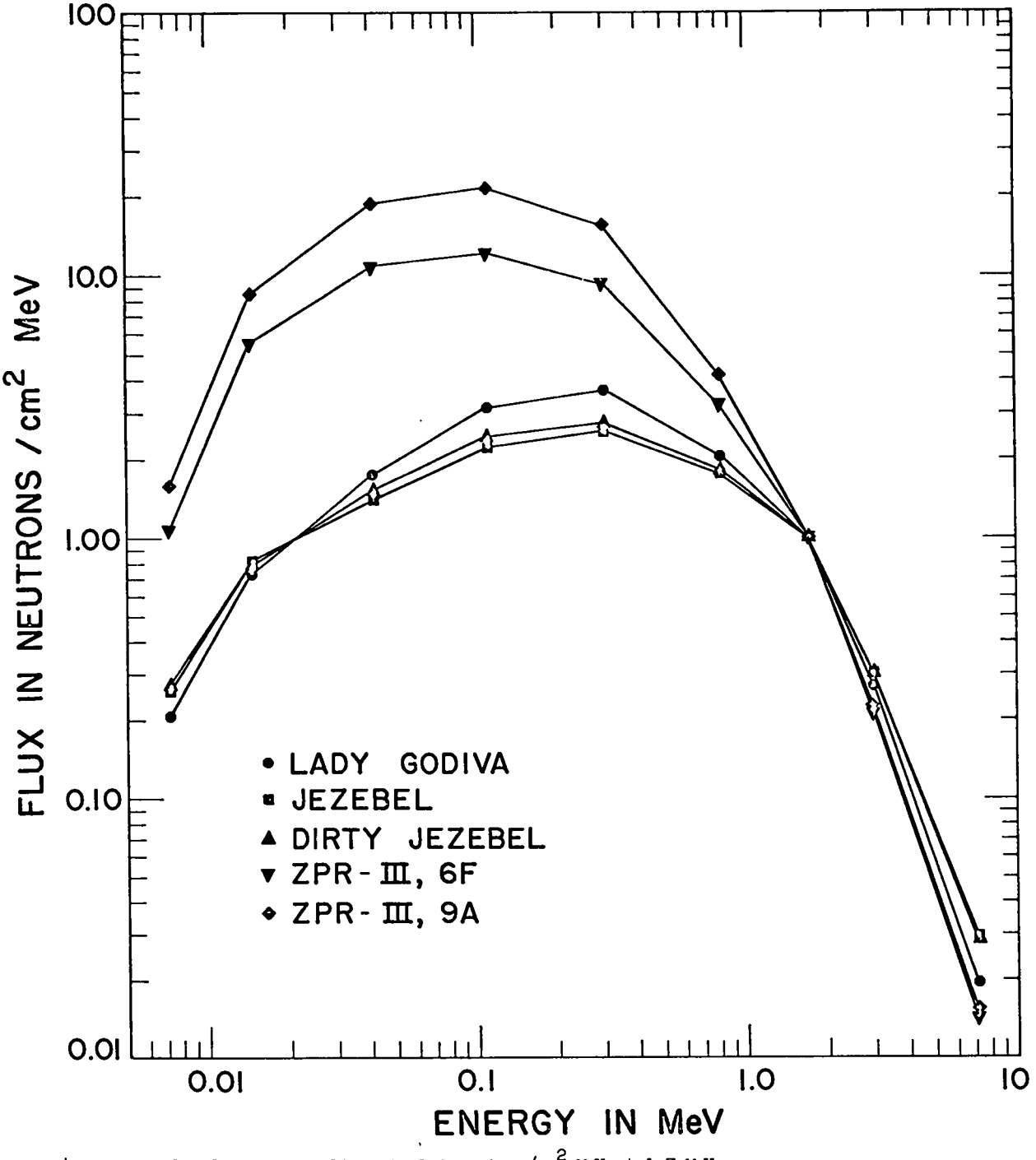

Figure 4. Assembly fluxes, normalized to 1.0 neutron/cm^2-MeV at 1.7 MeV.

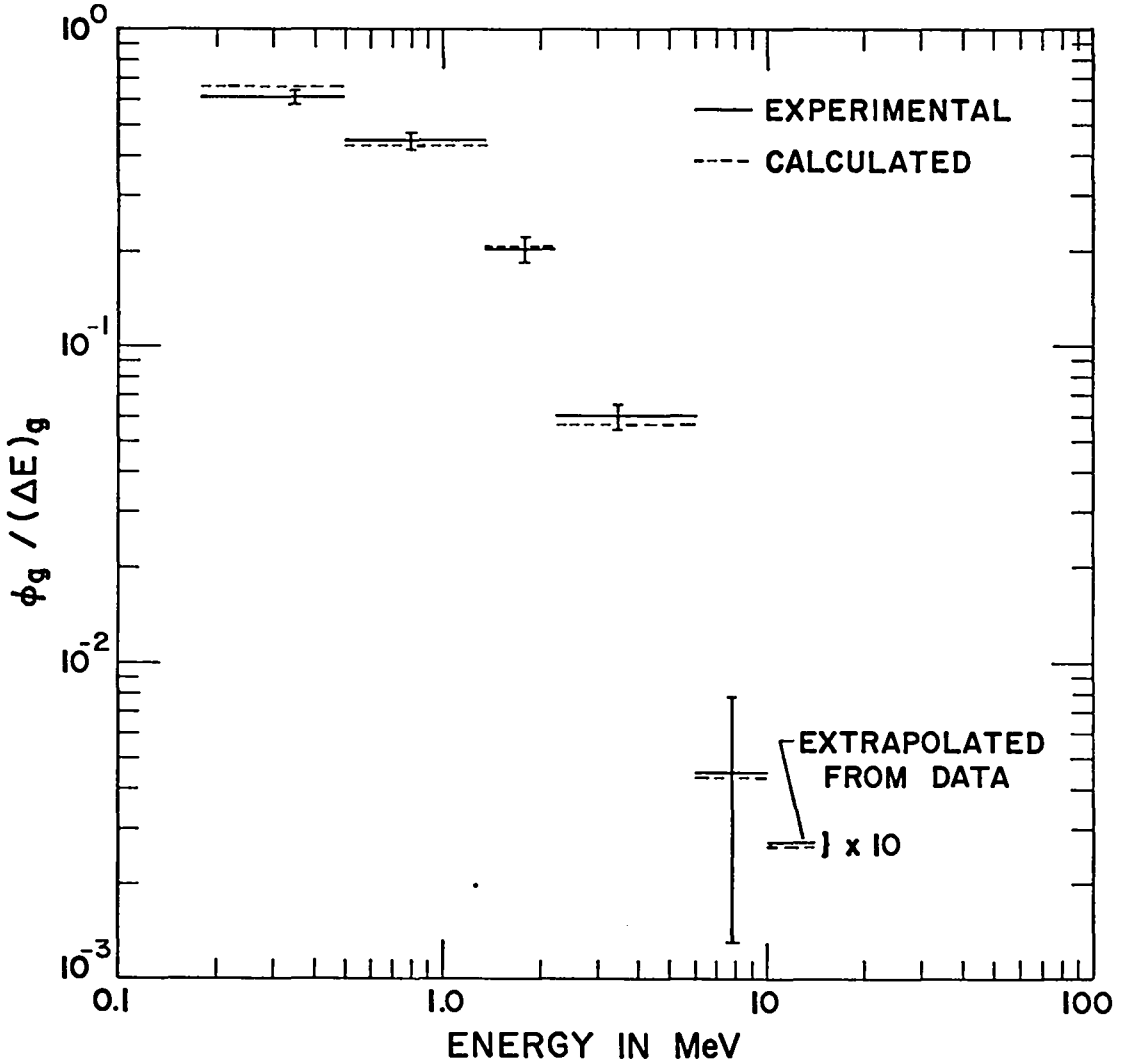

Figure 5. Leakage spectrum for Lady Godiva for first six groups. Both experimental and calculated spectra are normalized to 1.0 neutron/cm^2 over all six groups.

Note that the scaling could be applied to either detector or both. Correspondence with Russell[14] revealed an error in detector calibration. He agreed that our scaling was a reasonable treatment of the data.

The data of Profio et al.[13] are compared with those of Frye et al.[12] in Fig. 8. Note that the two experiments agree very well when the scale factor is applied to the data of Profio et al. Calculations indicate that the difference in spectra between a critical assembly such as Lady Godiva and a sphere with a multiplication near 20 should be very small.

The data of Profio et al.[13] have been integrated over the energy groups used in a 10-group S_n calculation. The calculated and observed spectra are compared in Fig. 9.

We mentioned above that the sensitivity of the calculations to variations in the cross sections is a function of the neutron flux. In addition, the flux spectrum is a very accurate indicator of such cross-section changes, and flux measurements provide one of the more sensitive tests of the relative merit of a given fit to cross-section data.

As an illustration of the usefulness of flux spectrum measurements, the data of Profio et al.,[13]

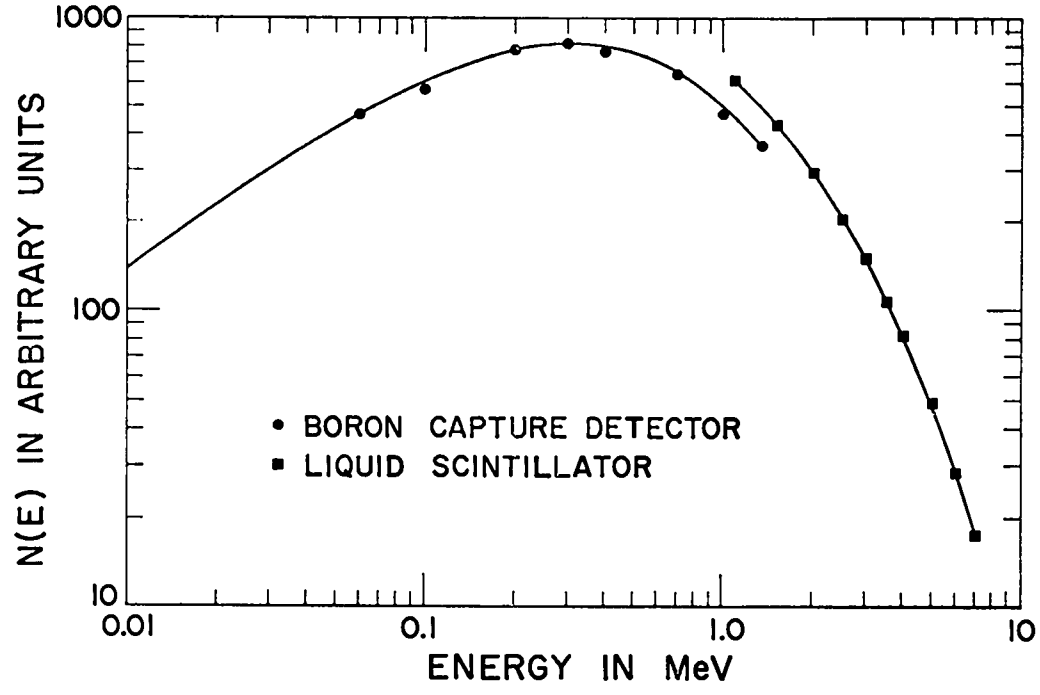

Figure 6. Leakage spectrum for enriched uranium, given in arbitrary units. Data are from Ref. 13, integrated over all angles.

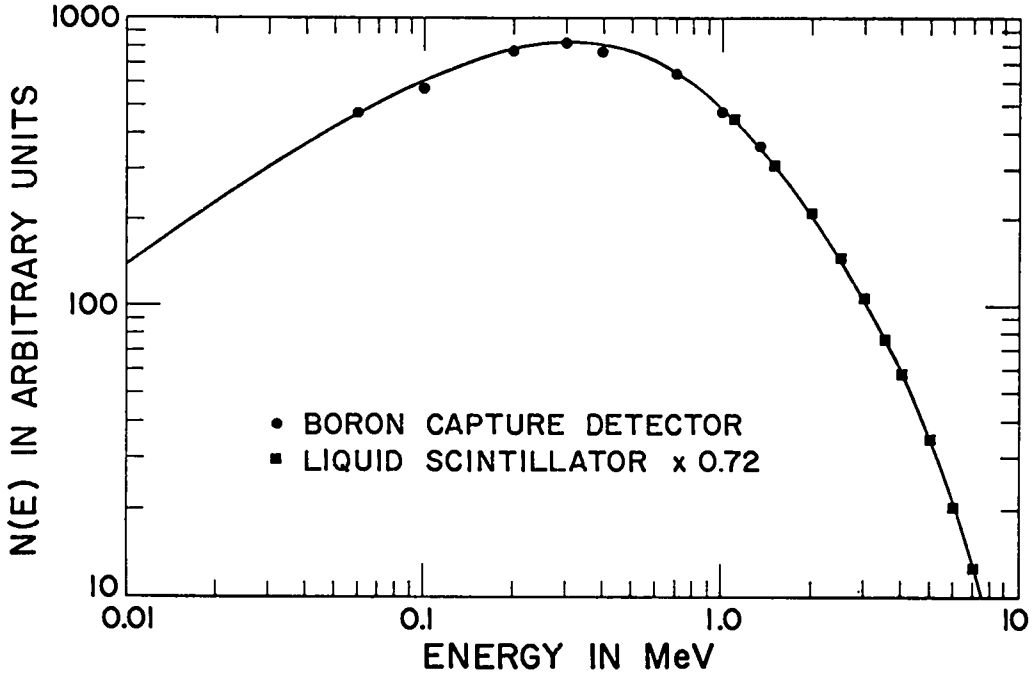

Figure 7. Leakage spectrum for enriched uranium, given in arbitrary units. Data are from Ref. 13, integrated over all angles; data for liquid scintillator are scaled by a factor of 0.72.

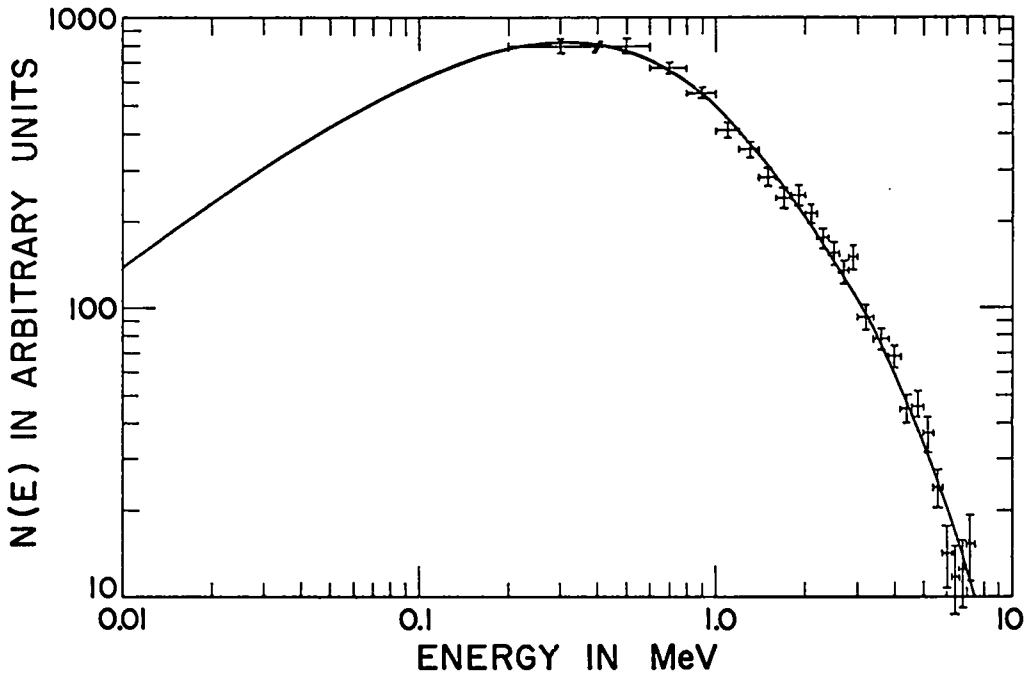

Figure 8. Leakage spectrum for enriched uranium, given in arbitrary units. Data of Refs. 12 and 13 are compared, with scale factor of 0.72 applied to the liquid scintillator data of Ref. 13.

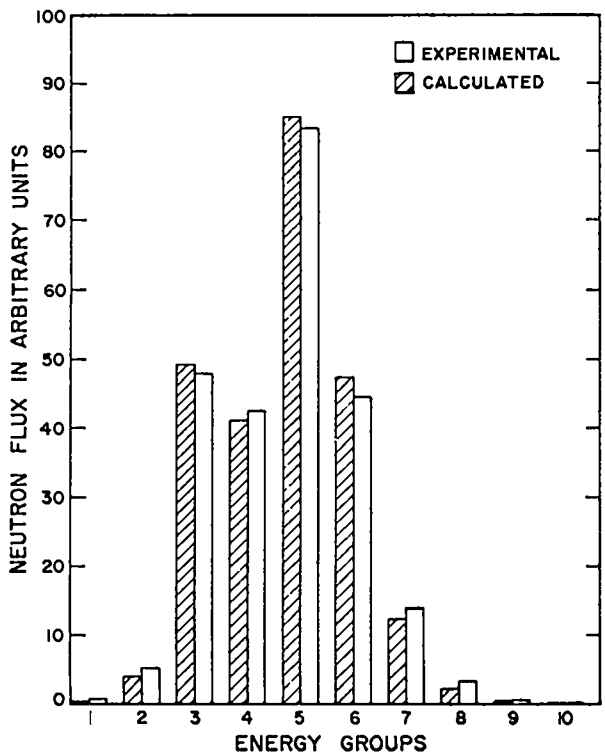

Figure 9. Leakage spectrum for enriched uranium, given in arbitrary units. Data of Ref. 13 are compared to calculated leakage spectrum.

particularly at lower energies, required us to change our specification of the final-state energy distribution for inelastic scattering to obtain the agreement shown in Fig. 9. After renormalization to the Lady Godiva assembly, the final set of cross sections as presented in Ref. 1 gave much better results in a number of other integral experiments.

The comparison of Jezebel leakage spectra with Stewart's[15] experimental data is shown in Fig. 10.

The usage of plutonium of varying isotopic compositions is increasing. Since it is of interest to understand the reactivity properties of plutonium as the composition is varied, we made a set of reactivity calculations at different compositions. The results are given as the calculated delayed-critical mass vs isotopic composition.

The concentration of each isotope for a given reactor exposure time is not a fixed value, being dependent on such quantities as the fuel composition and the neutron flux. For calculation, we took concentrations from data obtained by Barbieri et al.[16] in studies of the Calder Hall reactor. We added 1% of gallium to each sample. The six

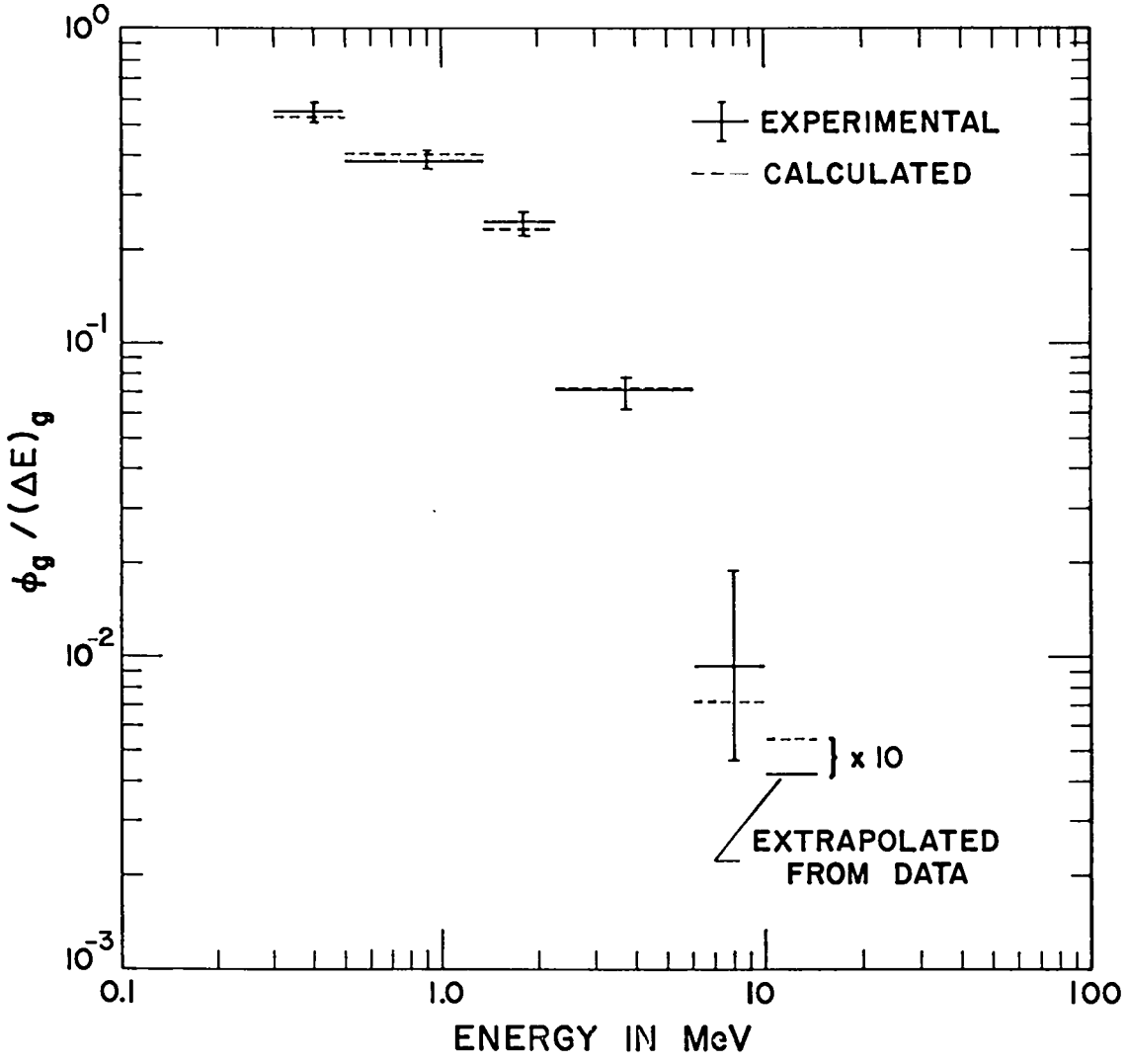

Figure 10. Leakage spectrum for Jezebel for first six groups. Both experimental and calculated spectra are normalized to 1.0 neutron/cm^2 over all six groups.

compositions chosen are:

1.	79.9% ^{239}Pu	3.	51.4% ^{239}Pu	5.	42.9% ^{239}Pu
	14.9% ^{240}Pu		23.8% ^{240}Pu		19.9% ^{240}Pu
	3.7% ^{241}Pu		15.9% ^{241}Pu		14.1% ^{241}Pu
	0.5% ^{242}Pu		7.9% ^{242}Pu		22.1% ^{242}Pu
	1.0% gallium		1.0% gallium		1.0% gallium
2.	65.4% ^{239}Pu	4.	46.3% ^{239}Pu	6.	39.7% ^{239}Pu
	23.3% ^{240}Pu		21.6% ^{240}Pu		19.2% ^{240}Pu
	8.0% ^{241}Pu		15.1% ^{241}Pu		13.9% ^{241}Pu
	2.3% ^{242}Pu		16.0% ^{242}Pu		26.2% ^{242}Pu
	1.0% gallium		1.0% gallium		1.0% gallium

These compositions make no allowance for the decay of ^{241}Pu, which has a 13-year half-life.

These calculations must be regarded as approximate, owing largely to the uncertainty in the ^{242}Pu cross sections and, to a lesser extent, the ^{241}Pu cross sections. The ^{241}Pu cross sections were taken largely from the compilation of Stehn et al.[17] Where data do not exist, we based the cross-section curves on our recommended curves[2] for ^{239}Pu.

The only data available on ^{242}Pu are fission cross sections reported by Butler[18] and Fomushkin et al.[19] Other ^{242}Pu cross sections were taken to be similar to the recommended curves for ^{240}Pu given in Ref. 2. The calculated delayed critical masses for the six isotopic compositions given above and for a constant density of 15.8 g/cm^3 are:

1. 17.97 kg
2. 19.68 kg
3. 21.17 kg
4. 23.02 kg
5. 24.57 kg
6. 25.83 kg

VI. CENTRAL CORE REPLACEMENT COMPARISONS

The reactivity contributions of a number of materials placed inside different critical assemblies have been measured experimentally. These contributions were measured by placing the materials in cavities in various locations in the assemblies. A control rod calibrated in units of mass added to the surface of the assembly is adjusted to bring the assembly to delayed critical. The reactivity contribution of a substance placed in the cavity is then determined from the amount of surface mass that must be added to obtain criticality. The surface mass that must be added to a delayed critical assembly to make it prompt critical is defined as one dollar (1\$). One percent of this mass is defined as one cent (1¢).

The change in reactivity of a system for a given change in the assembly mass was studied for central cavities. For both Lady Godiva and Jezebel the calculated change in reactivity was found to be proportional to the change in surface mass of the assembly. (The study was performed with changes in mass on the order of 1\$, with the system very near critical.) Thus the dollar can be defined equivalently as the reactivity change produced by the addition of the amount of surface mass, ΔM_c, required to bring the delayed critical assembly to prompt critical.

One can calculate the reactivity of an assembly at prompt critical, but including delayed neutrons. Then ΔM_c contributes an amount, Δk_c, to the reactivity, where Δk_c = k(prompt-critical mass) - k(delayed-critical mass). We can then define $\Delta k_c \equiv 1\$$. Since, by calculation, Δk is linear with ΔM, we can calculate the reactivity contribution of a sample by calculating the change in reactivity when a void in an assembly is filled with the sample material.

Experimentally, the reactivity contributions were measured using cylindrical samples 0.5 in. in diam. and 0.5 in. long. Because spherical symmetry is required for MODERN calculations, these samples were represented by a sphere of equal volume. The flux in such a small volume does not change rapidly, so the error introduced by this approximation should be small.

Table IV

REACTIVITY CONTRIBUTIONS

Material	Assembly	Exp. (¢/g-mole)	Calc. (¢/g-mole)
Oy (93.7% ^{235}U)	Lady Godiva	135.5	138.6
Oy (93.44% ^{235}U)	Jezebel	676.9	707.1
U(N)	Lady Godiva	21.9	17.5[a]
			20.3[b]
U(N)	Jezebel	94.4	86.9[a]
			91.9[b]
Pu (95.3% ^{239}Pu)	Jezebel	1424[c]	1429
^{239}Pu	Lady Godiva	279.6	281.9
^{240}Pu	Lady Godiva	168 ± 17	181
Beryllium	Lady Godiva	6.7	5.8
Beryllium	Jezebel	13.1	8.8
Carbon	Lady Godiva	2.2	2.7
Carbon	Jezebel	-5.8	-5.6
Iron	Lady Godiva	-0.1	-0.7
Iron	Jezebel	-18.1	-17.5
Tungsten	Lady Godiva	-3.6	-7.9
Tungsten	Jezebel	-60.9	-71.0

[a] Solid curve for σ_n, γ, ^{238}U, Fig. 11.
[b] Dotted curve for σ_n, γ, ^{238}U, Fig. 11.
[c] Corrected for gallium.

Table IV shows a comparison of the calculated reactivity contributions in the Lady Godiva and Jezebel assemblies with the experimentally observed values given by Engle et al.[20]

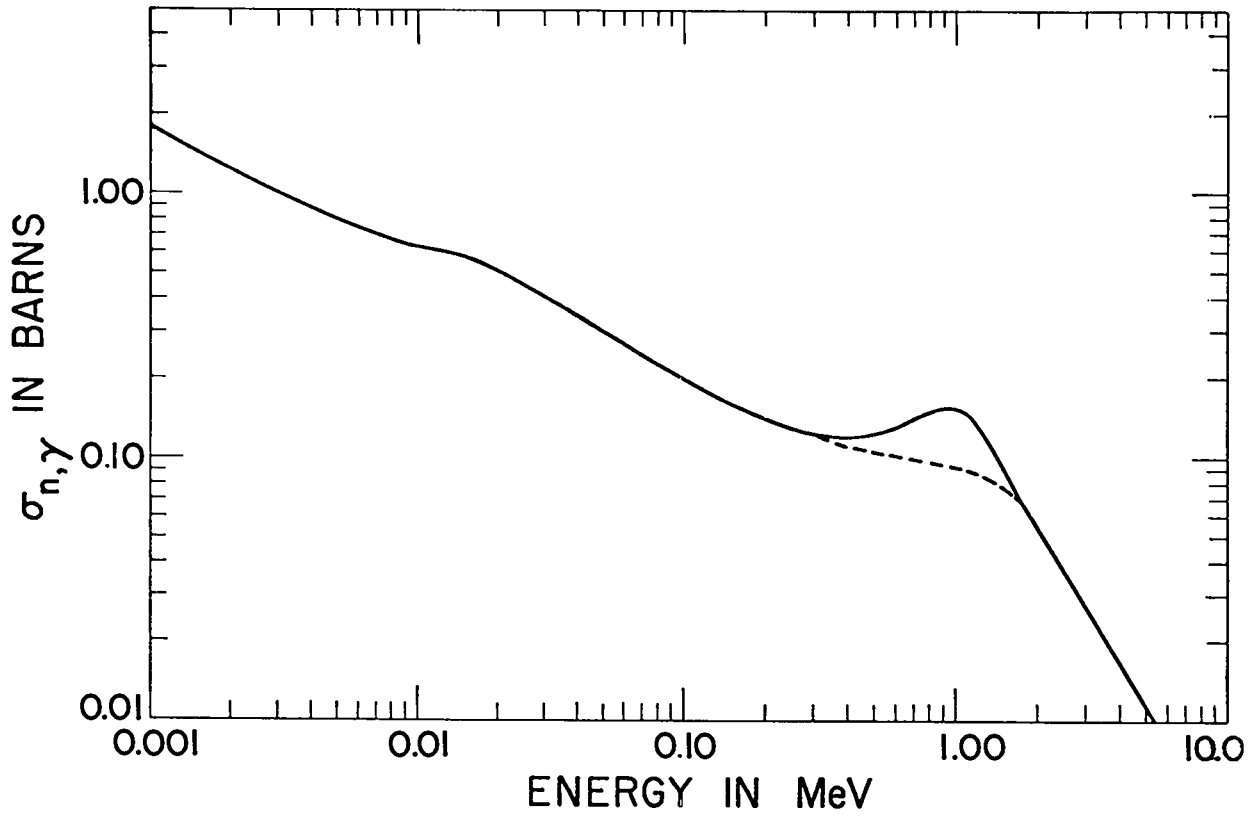

Figure 11. Radiative-capture cross section for ^{238}U, from Ref. 1. Solid curve is best fit to experimental data; dotted curve is recommended on the basis of calculations given in present report.

Figure 11 shows the radiative-capture cross section of ^{238}U, as presented in Ref. 1. The solid curve was used to obtain the values labelled by superscript "a" in Table IV. The calculated reactivity contributions of normal uranium are much lower than those measured. The dotted curve of Fig. 11 was used to calculate the values labelled by superscript "b," giving much better agreement with the experimental values of the reactivity contributions.

Agreement with experimental data is reasonably good, with the noticeable exception of the reactivity contribution of Oy in Jezebel. Many calculational studies were performed to gain insight into the source of this discrepancy, but without success. Although a calculational bias cannot be completely ruled out, it is considered unlikely in view of the number and widely varying types of materials reported in Table IV.

VII. SPECTRAL INDEX COMPARISONS

We define a spectral index by the quantity

$$\frac{\int \varphi_c(E)\sigma_{n,x_1}(A,Z,E)dE}{\int \varphi_c(E)\sigma_{n,x_2}(A',Z',E)dE} .$$

(n,x_1) and (n,x_2) can be any reaction. (A,Z) and (A',Z') may or may not be identical. The average is taken over the central flux of the assembly, so that a spectral index is dependent both on the cross sections involved and on the system flux. Experimentally, a spectral index is obtained by measuring the relative reaction rates of small samples located in the center of a critical assembly.

Experimental measurements of a wide range of spectral indices are summarized by Hansen,[9] Long et al.,[8] and Grundl and Hansen.[21] These measurements were performed in a variety of fast reactor assemblies, including Jezebel, Lady Godiva, ZPR-III,

Table V

COMPARISON OF SPECTRAL INDICES

Spectral Index	Flux Spectrum											
	^{235}U Fission Spectrum		Jezebel		Lady Godiva		U(N) Reflected Oy		ZPR-III Assembly 6F		ZPR-III Assembly 9A	
$\frac{\sigma_{n,f}(^{235}U)}{\sigma_{n,f}(^{238}U)}$	Exp.:	4.08	Exp.:	5.09	Exp.:	6.37	Exp.:	6.90	Exp.:	14.49	Exp.:	19.61
	Calc.:	4.48	Calc.:	5.53	Calc.:	6.84	Calc.:	7.53	Calc.:	14.44	Calc.:	20.14
$\frac{\sigma_{n,f}(^{239}Pu)}{\sigma_{n,f}(^{235}U)}$	Exp.:	1.54	Exp.:	1.47	Exp.:	1.42	Exp.:	1.42			Exp.:	1.25
	Calc.:	1.45	Calc.:	1.40	Calc.:	1.37	Calc.:	1.35	Calc.:	1.24	Calc.:	1.20
$\frac{\sigma_{n,\gamma}(^{238}U)}{\sigma_{n,f}(^{238}U)}$					Exp.:	0.476	Exp.:	0.53	Exp.:	1.217		
					Calc.:	0.575[a]	Calc.:	0.67[a]	Calc.:	1.471[a]		
	Calc.:	0.27[b]	Calc.:	0.38[b]		0.503[b]		0.58[b]		1.333[b]	Calc.:	1.96[b]
$\frac{\sigma_{n,\gamma}(^{238}U)}{\sigma_{n,f}(^{235}U)}$					Exp.:	0.075	Exp.:	0.0766	Exp.:	0.084		
					Calc.:	0.084[a]	Calc.:	0.0869[a]	Calc.:	0.102[a]		
	Calc.:	0.060[b]	Calc.:	0.068[b]	Calc.:	0.074[b]	Calc.:	0.0766[b]	Calc.:	0.092[b]	Calc.:	0.10[b]
$\frac{\sigma_{n,f}(^{237}Np)}{\sigma_{n,f}(^{235}U)}$	Exp.:	1.17	Exp.:	0.96	Exp.:	0.82	Exp.:	0.76				
	Calc.:	1.03	Calc.:	0.90	Calc.:	0.81	Calc.:	0.75	Calc.:	0.51	Calc.:	0.41
$\frac{\sigma_{n,f}(^{237}Np)}{\sigma_{n,f}(^{238}U)}$	Exp.:	4.28	Exp.:	4.69	Exp.:	5.22	Exp.:	5.24				
	Calc.:	4.64	Calc.:	4.97	Calc.:	5.53	Calc.:	5.64	Calc.:	7.36	Calc.:	8.31

[a] Solid curve for $\sigma_{n,\gamma}$, ^{238}U, Fig. 11.
[b] Dotted curve for $\sigma_{n,\gamma}$, ^{238}U, Fig. 11.

and a natural uranium [U(N)]-reflected Oy assembly. Measurements were also reported for a ^{235}U fission spectrum. The U(N)-reflected Oy reactor was a near-critical assembly containing approximately 8 in. of U(N). Averages of the experimental values and the calculated spectral indices are given in Table V. (The ^{237}Np fission cross sections were taken from the data of Schmitt and Murray.[22]) The calculated values are given only for the final recommended cross-section curves as presented in Refs. 1 and 2, except for the case of spectral indices involving $\sigma_{n,\gamma}$ for ^{238}U. Two sets of calculated indices involving this cross section are presented to show further the discrepancy between the experimental data on this cross section and the integral experiments. Again, the calculated values labelled "a" in Table V were based on the solid curve for $\sigma_{n,\gamma}(^{238}U)$, whereas those labelled "b" were based on the dotted curve for this cross section (See Fig. 11).

Agreement is obtained with all experimental values to within the experimental error (about ±10%), except for spectral indices involving $\sigma_{n,\gamma}(^{238}U)$ for the solid curve, where the difference is about 15 to 20%. Again, the agreement with experiment for these latter quantities is greatly improved by use of the dotted curve of Fig. 11.

We noted that if only the more recent values of Grundl and Hansen are used, differences between calculated and experimental values are increased by a few per cent, with the exception of $\overline{\sigma_{n,f}}(^{235}U)/\overline{\sigma_{n,f}}(^{238}U)$ in the ^{235}U fission spectrum where the difference is increased by 6%. Further, experimental accuracy in the recent measurements is improved, so that discrepancies may very well exist in the spectral index comparisons.

VIII. REFLECTED ASSEMBLY COMPARISONS

A number of critical assemblies in which a core of active material is surrounded by a reflector of inactive material have been studied experimentally. These assemblies are summarized in Table VI, using Paxton's[23] compilation of experimental data. (Composition of the graphite used as the reflector material in assemblies 11 through 14

Table VI

REFLECTED ASSEMBLIES

Assembly Number	Core			Reflector			
	Composition	Density (g/cm^3)	Mass (kg)	Material	Composition	Thickness (cm)	Density (g/cm^3)
1	93.9% ^{235}U 5.17% ^{238}U 0.93% ^{234}U	18.75	36.21	U(N)	0.73% ^{235}U 99.27% ^{238}U	1.765	19.0
2	93.9% ^{235}U 5.17% ^{238}U 0.93% ^{234}U	18.75	26.52	U(N)	0.73% ^{235}U 99.27% ^{238}U	4.473	19.0
3	93.9% ^{235}U 5.17% ^{238}U 0.93% ^{234}U	18.75	20.45	U(N)	0.73% ^{235}U 99.27% ^{238}U	8.954	19.0
4	93.9% ^{235}U 5.17% ^{238}U 0.93% ^{234}U	18.75	19.75	U(N)	0.73% ^{235}U 99.27% ^{238}U	9.970	19.0
5	93.2% ^{235}U 5.76% ^{238}U 1.04% ^{234}U	18.62	17.86	U(N)	0.73% ^{235}U 99.27% ^{238}U	18.009	19.0
6	93.9% ^{235}U 5.17% ^{238}U 0.93% ^{234}U	18.5	23.64	Beryllium	98% Beryllium 2% Oxygen	4.699	1.84
7	93.9% ^{235}U 5.17% ^{238}U 0.93% ^{234}U	18.75	23.0	Beryllium	98% Beryllium 2% Oxygen	4.801	1.84
8	93.6% ^{235}U 5.47% ^{238}U 0.93% ^{234}U	18.6	14.0	Beryllium	98% Beryllium 2% Oxygen	11.786	1.84
9	93.9% ^{235}U 5.17% ^{238}U 0.93% ^{234}U	18.6	31.63	Iron(cast)	95.2% Iron 2.55% Carbon 2.25% Silicon	5.08	7.16
10	93.9% ^{235}U 5.17% ^{238}U 0.93% ^{234}U	18.4	27.69	Iron(cast)	95.2% Iron 2.55% Carbon 2.25% Silicon	10.16	7.16
11	93.9% ^{235}U 5.17% ^{238}U 0.93% ^{234}U	18.7	31.52	Graphite	99.7% Carbon 0.05% Iron 0.01% Aluminum 0.24% Titanium	5.08	1.67
12	93.9% ^{235}U 5.17% ^{238}U 0.93% ^{234}U	18.7	25.88	Graphite	99.7% Carbon 0.05% Iron 0.01% Aluminum 0.24% Titanium	10.16	1.67
13	93.9% ^{235}U 5.17% ^{238}U 0.93% ^{234}U	18.45	22.90	Graphite	99.7% Carbon 0.05% Iron 0.01% Aluminum 0.24% Titanium	15.24	1.67
14	93.9% ^{235}U 5.17% ^{238}U 0.93% ^{234}U	18.75	20.77	Graphite	99.7% Carbon 0.05% Iron 0.01% Aluminum 0.24% Titanium	20.32	1.67

Table VI (continued)

REFLECTED ASSEMBLIES

Assembly Number	Core			Reflector			
	Composition	Density (g/cm^3)	Mass (kg)	Material	Composition	Thickness (cm)	Density (g/cm^3)
15	93.9% ^{235}U 5.17% ^{238}U 0.93% ^{234}U	18.75	25.67	Tungsten	90% Tungsten 7% Nickel 3% Copper	5.08	17.39
16	93.9% ^{235}U 5.17% ^{238}U 0.93% ^{234}U	18.75	20.66	Tungsten	90% Tungsten 7% Nickel 3% Copper	10.16	17.39
17	94.1% ^{239}Pu 4.9% ^{240}Pu 1% Gallium	15.79	8.48	U(N)	0.73% ^{235}U 99.27% ^{238}U	4.128	18.92
18	97.65% ^{239}Pu 1.35% ^{240}Pu 1% Gallium	15.74	6.28	U(N)	0.73% ^{235}U 99.27% ^{238}U	11.684	19.0
19	94.2% ^{239}Pu 4.8% ^{240}Pu 1% Gallium	15.52	5.97	U(N)	0.73% ^{235}U 99.27% ^{238}U	19.609	19.0
20	94.1% ^{239}Pu 4.9% ^{240}Pu 1% Gallium	15.79	8.48	Beryllium	98% Beryllium 2.0% Oxygen	3.688	1.83
21	94.1% ^{239}Pu 4.9% ^{240}Pu 1% Gallium	15.79	8.48	Tungsten	91.3% Tungsten 5.5% Nickel 2.5% Copper 0.7% Zirconium	4.699	17.21

was obtained from Orndoff.[24]) All assemblies specified are critical, so that k = 1.0 to within experimental error.

The calculated reactivities are given in Table VII, with the error in core mass expressed as an error in k. These values depend not only on the cross sections of the active isotopes, but also on the cross sections (particularly the scattering cross sections) of the reflector materials. Thus, discrepancies between calculated and experimental values may indicate errors in the cross sections of either the active or reflector materials or both.

As a final comparison of the two curves for the radiative-capture cross section in Fig. 11, we calculated the reactivities of the U(N)-reflected Oy assemblies using the two different sets of cross sections. These results are given in Table VIII and plotted in Fig. 12. No constant normalization of any other cross section, such as the ^{238}U fission cross section, could provide a relatively flat curve in Fig. 12 when the solid curve in Fig. 11 was being used to represent the capture cross

Table VII

CALCULATED REACTIVITIES FOR REFLECTED ASSEMBLIES

Assembly Number	Core Material	Reflector Material	Reflector Thickness (cm)	k (calc.)	Exp. Error
1	Oy	U(N)	1.765	1.000	± 0.001
2	Oy	U(N)	4.473	1.001	± 0.002
3	Oy	U(N)	8.954	1.000	± 0.003
4	Oy	U(N)	9.970	0.999	± 0.001
5	Oy	U(N)	18.009	1.000	± 0.001
6	Oy	Beryllium	4.699	1.007	± 0.002
7	Oy	Beryllium	4.801	1.008	-
8	Oy	Beryllium	11.786	0.995	± 0.004
9	Oy	Iron	5.08	1.008	± 0.005
10	Oy	Iron	10.16	1.026	± 0.008
11	Oy	Graphite	5.08	1.008	± 0.003
12	Oy	Graphite	10.16	1.015	± 0.002
13	Oy	Graphite	15.24	1.012	± 0.003
14	Oy	Graphite	20.32	1.015	± 0.004
15	Oy	Tungsten	5.08	1.002	± 0.002
16	Oy	Tungsten	10.16	0.999	-
17	Pu	U(N)	4.128	0.996	-
18	Pu	U(N)	11.684	1.006	-
19	Pu	U(N)	19.609	0.994	± 0.011
20	Pu	Beryllium	3.688	1.007	-
21	Pu	Tungsten	4.699	0.999	-

Table VIII

COMPARISON OF REACTIVITIES FOR U(N)-REFLECTED OY ASSEMBLIES

^{238}U Capture Cross Sections	Reflector Thickness (cm)				
	1.765	4.473	8.954	9.970	18.009
Solid Curve	0.9992	0.9988	0.9936	0.9919	0.9906
Dotted Curve	0.9995	1.0015	0.9997	0.9993	0.9999

section. The results are clearly outside the experimental errors on most of the assemblies.

However, when the dotted curve in Fig. 11 was used to represent the capture cross section, the resulting reactivity values are within experimental error for all assemblies. The dotted curve (or some equivalent variation) in Fig. 11 is thus indicated by a set of integral experiments.

In the study of reflected assemblies, we found that the initial best fit to experimental data in the Legendre expansion of the differential elastic scattering cross sections should be altered somewhat. In particular, the coefficients of $P_1(u)$ and $P_2(u)$ for ^{235}U were reduced to follow the lower data points, as shown in Fig. 13. The dotted curves show the original fits, while the solid curves are the final recommended values as given in Ref. 1. After renormalization of the fission cross section to the Lady Godiva assembly, these changes in the elastic scattering coefficients reduced the implied specific errors, $\frac{\Delta\Sigma}{\Sigma}$, by an amount of 2.6 to 3.7% in the cross sections of reflector materials. This corresponds to a reduction in the reactivity error, Δk, of from 0.0030 to 0.0075. The values were obtained for the various reflected assemblies listed in Table VI. (It should be remarked that an adjustment of the elastic scattering cross section by a corresponding amount would have produced the same effect.)

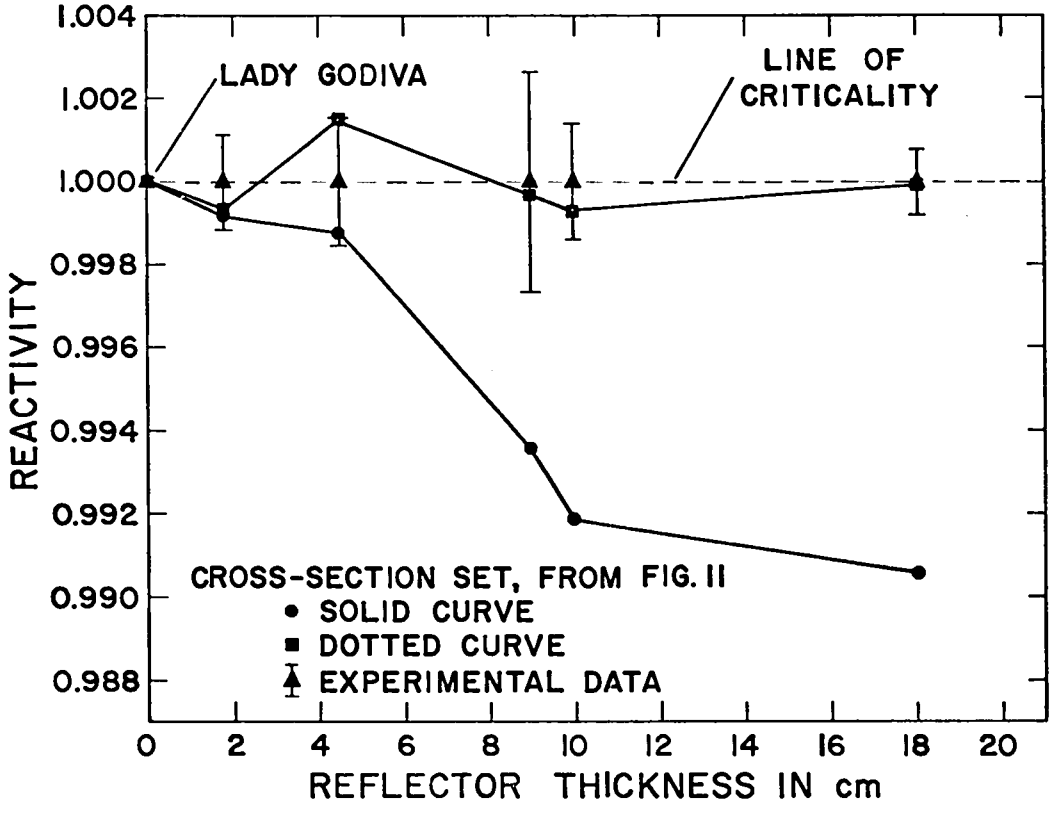

Figure 12. Reactivity vs reflector thickness for U(N)-reflected Oy. Upper curve is based on the dotted curve in Fig. 11; lower curve is based in the solid curve in Fig. 11.

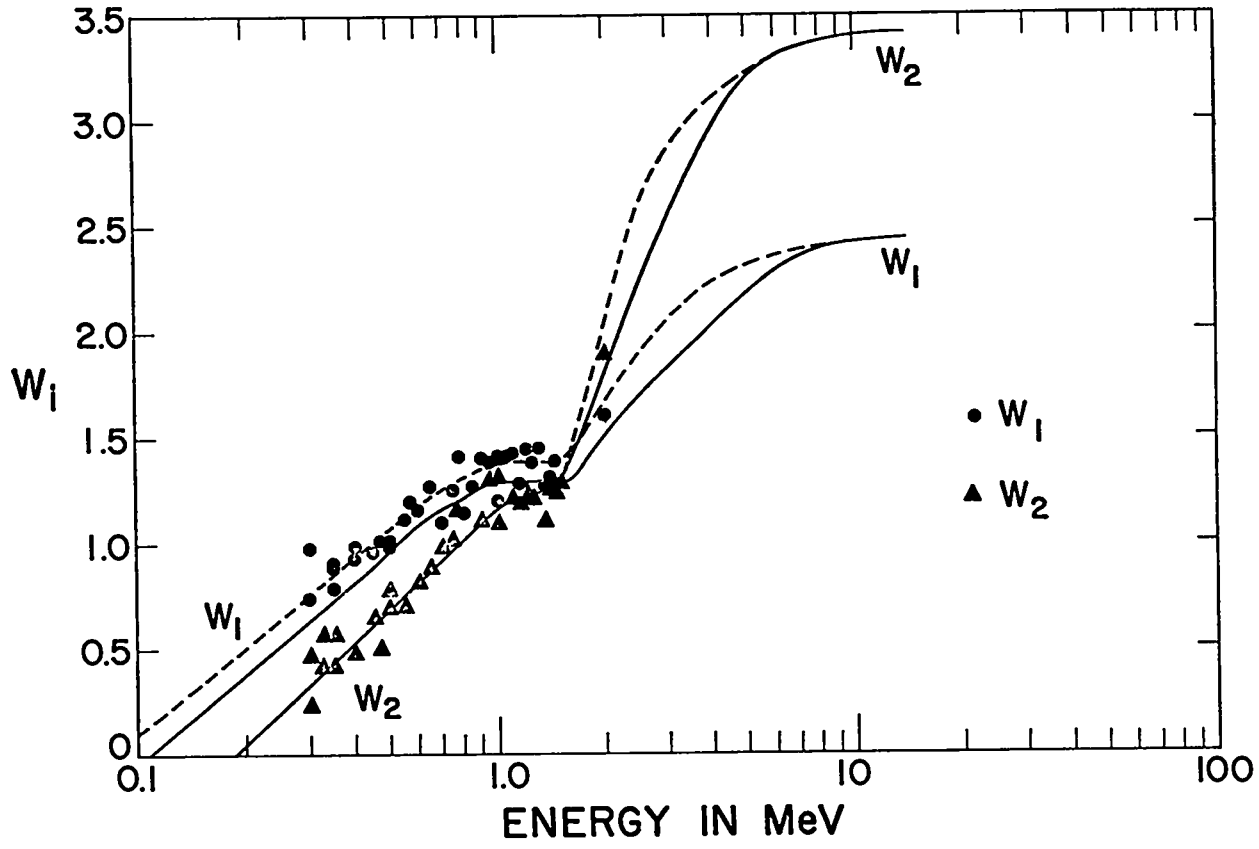

Figure 13. W_1 and W_2 Legendre coefficients for the differential elastic-scattering cross section of ^{235}U. Dotted curves are the initial best fits to the data; solid curves are the recommendations from Ref. 1.

The same Legendre expansion was used for ^{239}Pu and ^{240}Pu (see Ref. 2), for which very few data exist.

IX. SUMMARY

A wide range of integral comparisons have been reported. Based on these comparisons, the microscopic cross-section curves recommended for neutronics calculations of fast critical assemblies were established[1,2] for ^{235}U, ^{238}U, ^{239}Pu and ^{240}Pu. In view of the range of experiments and the generally good agreement between the calculated values and the experimental data, we feel that the recommended cross-section curves can be used with confidence within the limits set by the fluxes of the systems that were studied.

Obviously a set of cross sections as a function of energy theoretically represents an infinite set of parameters that can be adjusted in an infinite number of ways to obtain agreement with a finite set of integral values. That continuity between energy points was required, and that some physical theory and understanding were applied in making these adjustments, reduces the number of possible sets considerably; nevertheless, care should be exercised in using these evaluations on assemblies whose fluxes and neutronic characteristics lie outside the range studied in this report.

ACKNOWLEDGMENTS

We gratefully acknowledge the many helpful discussions held with G. E. Hansen, J. A. Grundl, and H. C. Paxton of LASL Group N-2, and with K. F. Famularo and C. P. Cadenhead of Group W-4. Leona Stewart of P-DOR and B. C. Diven of Group P-3 very kindly assisted in providing both data and data evaluation for the program, and G. H. Best of Group K-1 provided data on reactor characteristics. We also acknowledge the invaluable assistance of P. P. Whalen of Group W-4 in writing the computer codes

used in the program, and that of C. Foglesong of Group W-4 in performing many of the calculations. Finally, we thank Nora Rodgers and Lucy Henson of Group W-4 for their efforts in the preparation of this report.

REFERENCES

1. J. -J. H. Berlijn, R. E. Hunter, and C. C. Cremer, "Neutron Cross Sections for ^{235}U and ^{238}U in the Energy Range 1 keV to 14 MeV," LA-3527 (1968).

2. R. E. Hunter, J. -J. H. Berlijn, and C. C. Cremer, "Neutron Cross Sections for ^{239}Pu and ^{240}Pu in the Energy Range 1 keV to 14 MeV," LA-3528 (1968).

3. C. E. Lee, "The Discrete S_n Approximation to Transport Theory," LA-2595 (1962).

4. B. G. Carlson and K. D. Lathrop, "Transport Theory - The Method of Discrete Ordinates," LA-3251-MS (1965).

5. R. E. Peterson, "Lady Godiva - An Unreflected Uranium-235 Critical Assembly," LA-1614 (1953).

6. G. A. Jarvis, G. A. Linenberger, and H. C. Paxton, "Plutonium-Metal Critical Assemblies," LA-2044 (1956).

7. D. M. Barton, LASL Group N-2, private communication (1965).

8. J. K. Long, W. B. Loewenstein, C. E. Branyan, G. S. Brunson, F. S. Kirn, D. Okrent, R. E. Rice, and F. W. Thalgott, "Fast Neutron Power Reactor Studies with ZPR-III," Proc. UN Intern. Conf. Peaceful Uses At. Energy, 2nd, Geneva, 1958, paper No. 598 (1958).

9. G. A. Jarvis, G. A. Linenberger, J. D. Orndoff, and H. C. Paxton, "Two Plutonium-Metal Critical Assemblies," Nucl. Sci. Eng. 8, 525 (1960).

10. G. E. Hansen, "Status of Computational and Experimental Correlations for Los Alamos Fast-Neutron Critical Assemblies," Physics of Fast and Intermediate Reactors, Vol. 1, IAEA, Vienna (1962), p. 445.

11. P. J. Bendt, H. J. Karr, and F. R. Scott, "Alpha Measurements of the Godiva Critical Assembly Using a Betatron," LA-1515 (1953).

12. G. M. Frye, Jr., J. H. Gammel, and L. Rosen, "Energy Spectrum of Neutrons from Thermal Fission of U^{235} and from an Untamped Multiplying Assembly of U^{235}," TID-10073 (1954).

13. A. E. Profio, J. C. Young, K. L. Crosbie, R. Hackney, H. M. Antunez, and J. L. Russell, Jr., "Time-of-Flight Measurements of Neutron Spectra in U^{235} and Tungsten," G. A. -7427 (1966); Trans. Am. Nucl. Soc. 9, 233 (1966).

14. J. L. Russell, Jr., Gulf General Atomic, Inc., private communication (1967).

15. L. Stewart, "Leakage Neutron Spectrum from a Bare Pu^{239} Critical Assembly," Nucl. Sci. Eng. 8, 595 (1960).

16. L. Barbieri, J. Webster, and K. Chow, "Plutonium Recycle in the Calder Hall Type Reactor," Nucl. Sci. Eng. 5, 105 (1959).

17. J. R. Stehn, M. D. Goldberg, R. Wiener-Chasman, S. F. Mughabghab, B. A. Magurno, and V. M. May, "Neutron Cross Sections," BNL-325, 2nd Ed., Suppl. No. 2 (1965).

18. D. K. Butler, "Fission Cross Section of Plutonium - 242," Phys. Rev. 117, 1305 (1960).

19. E. F. Fomushkin, E. K. Gutnikova, Yu. S. Zamyatnin, B. K. Maslennikov, V. N. Belov, V. M. Surin, F. Nasyrov, and N. F. Pashkin, "Cross Sections and Fragment Angular Anisotropy in Fast-Neutron Fission of Some Isotopes of Plutonium, Americium, and Curium," Sov. J. Nucl. Phys. 5, 689 (1967); Yadern. Fiz. 5, 996 (1967).

20. L. B. Engle, G. E. Hansen, and H. C. Paxton, "Reactivity Contributions of Various Materials in Topsy, Godiva, and Jezebel," Nucl. Sci. Eng. 8, 543 (1960).

21. J. A. Grundl and G. E. Hansen, "Measurement of Average Cross-Section Ratios in Fundamental Fast-Neutron Spectra," LA-DC-7851 (1966).

22. H. W. Schmitt and R. B. Murray, "Neutron-Induced Fission Cross Section of Np^{237}," Phys. Rev. 116, 1575 (1959).

23. H. C. Paxton, "Los Alamos Critical-Mass Data," LAMS-3067 (1964).

24. J. D. Orndoff, LASL Group N-2, private communication (1965).

ERRATA FOR LA-3527 AND LA-3528

Since the publication of the previous two reports in this series, LA-3527 and LA-3528, a number of typographical errors in those reports have come to our attention. The following corrections should be made to copies of those reports.

LA-3527

p. 7 - Section H

The third equation for $\bar{\nu}$ should read

$$\bar{\nu} = 2.898 + 0.098E \text{ (MeV)},$$
$$8.0 \leq E \leq 14 \text{ MeV}.$$

p. 8 - Eq. (8) should read

$$\frac{d\sigma_{n,n}}{d\Omega} = \frac{\sigma_{n,n}}{4\pi}\left[1 + \sum_{i=1}^{10} W_i P_i(u)\right],$$

p. 12 - Table II

$\sigma_{n,F}$ at 1.5 MeV should read 0.330.

LA-3528

p. 6 - Eq. (5) should read

$$F(E) = \frac{E}{T^2} e^{-E/T},$$

p. 8 - Section K

In the third sentence, ^{238}U should be ^{235}U.

p. 25 - Figure 14

The vertical scale should run from 0.01 to 100.0 instead of from 0.1 to 1000.0.